Theory of Tackiness

Cyprien Gay* and Ludwik Leibler†

Laboratoire CNRS–Elf Atochem (UMR 167), 95, rue Danton, B.P. 108, 92303 Levallois-Perret cedex, France
(Received 15 April 1998)

We show that the interplay between surface roughness on micron scale and air suction can yield tack energies much higher than thermodynamic surface energies. Our model provides a quantitative interpretation of highly nonlinear force-versus-separation curves which are usually observed when adhesion forces and energies are high. [S0031-9007(99)08393-3]

A substance appears sticky when some work is required to remove one's finger from it. This property is known as tackiness. Day-to-day examples are very numerous and usually involve polymer films. Controlling the tackiness of materials is important in many applications. For example, in pressure-sensitive adhesives a high tackiness is desired, whereas, conversely, coatings and paints, which are made roughly from the same polymers, should not be sticky. The feeling of tackiness is due both to the high energy dissipated during the bonding-debonding cycle, and to the high force required to separate the probe (finger) from the polymer film. In some case, the tack energy can be very high, up to 10^4 times as large as the thermo-dynamic Dupré work W associated with the difference in surface energies. Qualitatively, this high tack energy has been associated with a strong viscoelastic dissipation in the polymer film [1,2]. From the large body of experiments, two situations can be distinguished: either the dissipation is mainly due to a fracture that propagates along the substrate [3–5] or it arises through a much more complex mechanism where the polymer film is split into separate filaments or fibrils during the debonding process [6]. It appears that in many situations where fibrillation occurs during debonding, the traction curves obtained [7] from reproducible experiments (where a metallic probe is used rather than a finger) resemble that presented on Fig. 1. In the experiments, the separation rate is kept constant. The measured force presents a strong peak to start with, and then does not fall to zero, but rather stays essentially constant or rises slightly, till the probe finally separates from the film at a relatively high deformation. Both the maximum stress π_{max} and the tack energy G (area below the curve) can be very high. The reason for such a shape of the traction curve is still a mystery, and more generally, the values of the maximum stress and of the tack energy are not explained quantitatively.

The aim of the present Letter is to describe a mechanism for the very nonlinear behavior of the film during debonding. For the first time, it takes into account the role of air bubbles at the interface to give quantitative predictions for the value of the maximum traction force, for the plateau value and for the tack energy G, in the case of an elastic material.

It has been observed for a long time that the surface roughness of the solid probe greatly affects the tack energy [8], and this was attributed to the restriction of the true area of contact with the polymer film [8,9] during the bonding stage. Indeed, tacky polymeric materials are usually soft (typical modulus value 10^5 Pa [1]). Thus, the van der Waals surface forces alone are able to deform the polymer film surface and an intimate contact can be achieved, despite the probe surface roughness. We show that the roughness can also provide an explanation for the stress peak. Indeed, air bubbles can be trapped at the interface and lead to a "suction-cup" effect. We also show that the resulting adhesion reinforcement can cause fractures to propagate inside the material, thus creating fibrils. The stress at the fracture head is constant during propagation, and this accounts for the stress plateau in the traction curve. In the present model, we assume that the material is purely elastic: it is supposed to be incompressible, and it is characterized by its elastic modulus E and by the maximum tensile stress τ_f it can withstand before it starts to fracture. Our approach is
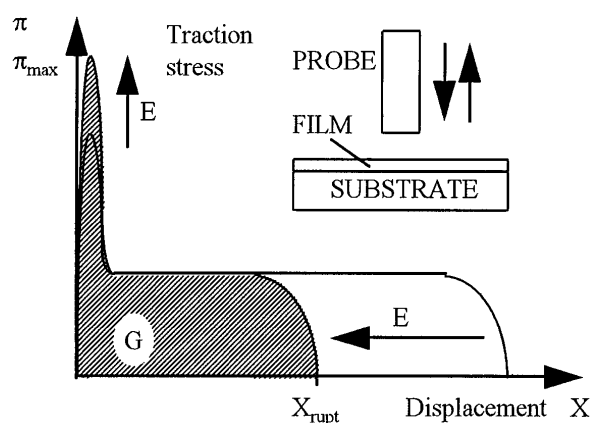
FIG. 1. Typical stress curve observed (Ref. [7]) at imposed displacement (constant separation rate). The traction force increases sharply upon separation. It then strongly decreases again and reaches a plateau, until it decreases further to zero. Our model predicts that the plateau should shorten and that the peak should increase with increasing modulus E (see Fig. 5). Inset: Usual experimental geometry.

    0031-9007/99/82(5)/936(4)$15.00

restricted to scaling laws: numerical factors are omitted in most formulas.

When two materials are brought into contact, their surface roughnesses are crucial to determine the quality of contact and hence the intensity of adhesion. Because of the nonconformity of the surface shapes brought into contact, the true area of contact is not equal to the nominal one. For deformable solids, the true area of contact depends strongly on the pressure applied to maintain the contact and on the attractive surface forces (e.g., van der Waals interactions W).

Indeed, even in the absence of external pressure (load), the surface forces are able to deform soft solids on the length scale of the roughness, and the area of contact in nonzero [8–10]. For rigid materials, the true area of contact is restricted to the summits of the rough surfaces. When $E \approx E^\star \equiv WD/\Sigma^2$ (where Σ is the roughness amplitude, and D its typical wavelength), the true area of contact is of order of half the nominal area of contact, and therefore it saturates [9] when $E \leq E^\star$. In the present approach, we are interested in the soft regime $E \leq E^\star$, and we argue that yet another phenomenon takes place, namely, the formation of air bubbles: the contact between both materials includes, in particular, the saddle points, and thus causes air to be trapped [11].

Typical values for the roughness of a metallic probe [8] are $\sigma \simeq 1~\mu$m (amplitude) and $d \simeq 10~\mu$m (wavelength). The corresponding radius of curvature of the asperities and hollows is of order $d^2/\sigma \simeq 100~\mu$m. The surface roughness of the polymer film plays an important role as well [12]. It strongly depends on the formation and coating procedures. For our purpose, we shall take the following estimation: film roughness amplitude $\Sigma = 5~\mu$m and wavelength $D = 100~\mu$m, corresponding to a radius of curvature of order $D^2/\Sigma \simeq 2$ mm. Taking $W = 5 \times 10^{-2}$ J/m^2 as the Dupré energy, we see that typical values $E \simeq 2 \times 10^4$ Pa for the polymer elastic modulus are below both critical values $E^\star_{\text{probe}} \equiv Wd/\sigma^2 \simeq 5 \times 10^5$ Pa and $E^\star_{\text{film}} \equiv WD/\Sigma^2 \simeq 2 \times 10^5$ Pa. In the present case of soft films ($E < E^\star_{\text{probe}}$ and $E < E^\star_{\text{film}}$), two populations of bubbles appear (Fig. 2, bottom left). Macrobubbles are induced by the long wavelength of the film roughness. They are surrounded by a continuous contact zone which contains microbubbles induced by the shorter wavelength of the probe roughness ($d < D$).

Because of both roughnesses, the contact between the probe and the film is very nonhomogeneous. In order to describe the resulting complex behavior, it is necessary to describe first the response of the contact zone around the macrobubbles and therefore to understand the role of the microbubbles. We therefore determine below how the local displacement x, taken at some distance δ away from the microbubbles ($\delta > d$, so that the nonhomogenities due to the microbubbles are averaged out), is related to the stress τ at the same point. The bubble width B_μ and
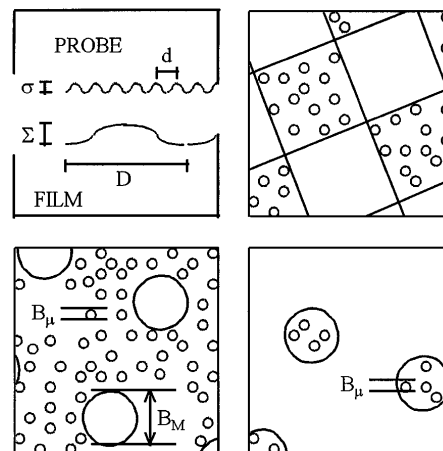
FIG. 2. Interface geometry. When the probe and film surface roughnesses combine, two populations of bubbles are present at the interface (left): macrobubbles (diameter B_M) originate in the film roughness (larger wavelength D), and microbubbles (diameter B_μ) are due to the roughness of the metallic probe (wavelength d). The area of contact around the macrobubbles is continuous and contains microbubbles. During traction, macrobubbles widen and finally merge (percolation, top right). Air is then pumped in (suction), and there remain contact spots that include microbubbles (bottom right).

depth β_μ result from a balance between different effects: air compression or expansion inside the bubble, elastic deformation of the polymer film around the bubbles and surface forces. These components can be summarized in the following free energy:

$$F \simeq \int_{\omega_0}^{\omega} (p_0 - p)d\omega + B_\mu^3 E(\beta_\mu/B_\mu)^2 + WB_\mu^2. \quad (1)$$

The first term describes the compression of air from the atmospheric pressure p_0 to $p = p_0\omega_0/\omega$ when the initial volume $\omega_0 \simeq \sigma d^2$ is changed to the current bubble volume ω. The volume $\omega \simeq \beta_\mu B_\mu^2$ is directly related to the mesoscopic displacement x if the polymer is incompressible: $\omega = \omega_0 + d^2 x = \omega_0(1 + x/\sigma)$. The bubble depth β_μ is much greater than the initial bubble depth σ. Hence, the material that surrounds the bubble can be modeled as a flat polymer sample penetrated by a hard sphere of radius B_μ^2/β_μ over a distance β_μ. Hence, for small deformation [10] ($\sigma \ll \beta_\mu \ll B_\mu$), the elastic energy (second term) is roughly that of a volume B_μ^3 deformed by a factor β_μ/B_μ. The third term accounts for surface interactions (W is the Dupré energy that is gained per unit surface area when the contact is formed).

Suppose now that traction is being performed locally in a quasistatic manner. At any imposed position x, the compression energy [first term of Eq. (1)] is fixed. Minimizing the remaining two terms with respect to B_μ, keeping $B_\mu^2\beta_\mu = \omega = \omega_0(1 + x/\sigma)$ fixed, yields the bubble diameter and the resulting mesoscopic stress:

$$B_\mu(x) \simeq d(E/E^\star_{\text{probe}})^{1/5}(1 + x/\sigma)^{2/5}, \quad (2)$$

$$\tau = \frac{1}{d^2}\frac{dF}{dx} \simeq p_0\left[\frac{x/\sigma}{1 + x/\sigma} + \frac{(E/E^-)^{2/5}}{(1 + x/\sigma)^{1/5}}\right], \quad (3)$$

where

$$E^- \equiv p_0^{5/2}\sigma^{1/2}d/W^{3/2}. \quad (4)$$

The first term of Eq. (3) accounts for the fact that increasing the bubble volume through traction amounts to working against the atmospheric pressure. The second term corresponds to the elastic deformation of the polymer that surrounds the bubble. The shape of the local response that corresponds to Eq. (3) presents a stress maximum,

$$\tau_0 = p_0[1 + (E/E^-)^{1/2}]. \quad (5)$$

Equation (2) shows that the microbubbles widen. At some point after the stress maximum, the bubble dimension reaches $B_\mu(x) \approx d$ and the microbubbles merge (reverse percolation of the area of contact).

Let us now impose a macroscopic traction displacement $X > 0$. It is mainly absorbed by the (weaker) macrobubbles, which thus increase in size $[\Omega = \Omega_0(1 + X/\Sigma)]$. First, the macrobubbles swell (β_M increases) but do not widen. The local stress increases correspondingly in the vicinity of the microbubbles: $\tau^\star \simeq E\beta_M/B_M$. At some point, $\tau^\star$ reaches the maximum of the local traction curve [Eqs. (3) and (5)]. At this point, the evolution of those microbubbles located in the vicinity of a macrobubble is unstable since they are subjected to the imposed stress $\tau^\star \geq \tau_0$ (rather than imposed displacement x): the microbubbles therefore merge (see Fig. 3). The film thus locally debonds from the probe and the macrobubbles widen (B_M increases). The macrobubble evolution is stable, however. Indeed, at any imposed position X, if the microbubble diameter B_M were becoming too large, the local stress $\tau^\star \simeq E\beta_M/B_M = \Omega(X)/B_M^3$ would decrease below τ_0, thus preventing any further local debonding and B_M increase.

Hence, the local stress is fixed ($\tau^\star \simeq \tau_0$) and the bubble dimensions are deduced from the fixed volume condition $[\beta_M B_M^2 = \Omega = \Omega_0(1 + X/\Sigma)]$. Eventually, at some displacement X_{pop} (such that $B_M \approx D$), the macrobubbles get connected. The air pressure is smaller inside the bubbles than outside, since their volume Ω is increased. Hence, air is pumped into the macrobubbles when $X = X_{pop}$ and causes a weak "pop" sound, similar to the behavior of a suction cup. Clearly, the bubble volume and shape are different at this stage ($X = X_{pop}$) from what they were at the initial contact $X = 0$ (for instance, $\beta_M > \Sigma$), and that is one source of irreversibility.
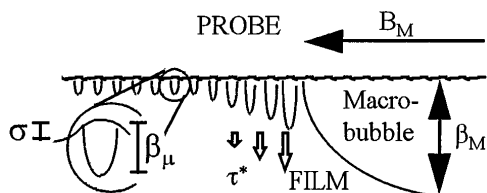
The whole process is thus accompanied by high stress inhomogeneities. Yet one can argue that at the percolation threshold, the bubbles and their vicinity represent virtually the whole nominal surface. Hence, the macroscopic stress at suction (Fig. 2, top right) is just slightly weaker than the local stress near the macrobubbles: $\pi \equiv \tau^\star/\kappa$, where κ is a numerical factor that depends on the detailed geometry (κ is somewhat larger than unity, say, $\kappa \simeq 2$). As we now show, if the polymer can fracture above some stress τ_f that is slightly lower than τ_0 (namely, $\tau_0/\kappa < \tau_f < \tau_0$), the above surface debonding mechanism is followed by a regime of fracture propagation. Consider a region of the wavy surface (Fig. 4, top). The most likely location of a fracture initiation is at point F_3, i.e., in the valley around a contact spot. Indeed, the polymer is laterally stretched at point F_3, which is not the case at points F_1 and F_2. Conversely, nothing happens before the reverse percolation has taken place: on the one hand, the stress is insufficient at the sample side for a horizontal, cohesive fracture to initiate ($\pi_{max} = \tau_0/\kappa < \tau_f$); on the other hand, there is no preferential direction for fracture opening at a bubble center F_3 (Fig. 4, bottom), even though the stress intensity $\tau^\star$ may be sufficient there. Once suction has occurred, however, fractures will initiate along the valleys between neighboring peaks (see Fig. 4, top). Fractures then propagate vertically through the film thickness. The stress at the fracture tip is equal to τ_f once it has started. The

FIG. 3. Mechanism for macrobubble widening. The stress $\tau^\star$ around the macrobubble tends to swell the surrounding microbubbles. If it exceeds the value τ_0, these microbubbles merge and open into the macrobubble. Vertical dimensions are overmagnified.
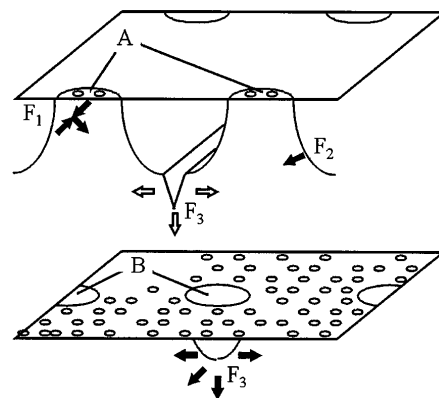
FIG. 4. Conditions for fracture initiation. Note that the amplitude of roughness has been magnified for clarity. Top: The various components of the stress tensor make it more favorable for a fracture to start along the valley lines between contact spots A (point F_3) than elsewhere at the interface (F_1 or F_2). Bottom: Before the reverse percolation has taken place, however, there is no preferential direction for fracture initiation in the bubbles B and fracture cannot start, even though the stress intensity could be sufficient.
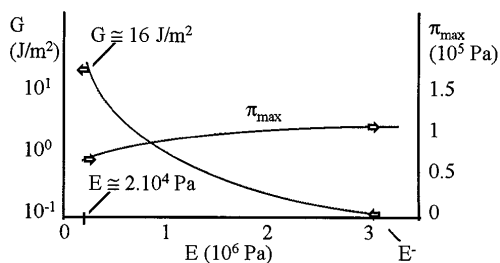
FIG. 5.   Predictions of the model, using the parameter values given in the text, and taking $\tau_f = $ const. The tack energy G has a strong dependence on the elastic modulus E, whereas the traction peak π_{max} varies mildly.

macroscopic traction stress is then $\pi \simeq \tau_f/\kappa$. Hence, the fracture initiation, which occurs just after suction in this case, causes a sudden decrease in the traction stress from $\pi \approx \tau_0/\kappa$ to $\pi \approx \tau_f/\kappa$, and that is the reason for the peak in the stress curve. The stress at the contact spots also decreases (from $\tau^\star \simeq \tau_0$ to $\tau^\star \simeq \tau_f$), and is thus lower than that required for further detachment of the polymer from the probe ($\tau^\star \cong \tau_f < \tau_0$). Hence, the contacts remain firmly attached thanks to the reinforcing presence of the microbubbles, and the fractures propagate further as the probe is being pulled back. They progressively create fibrils. Propagation stops when the fracture heads reach the solid substrate on the opposite side of the film. During fracture propagation, the part of the film that is turned into fibrils is thus elongated by a factor τ_f/E. The displacement corresponding to complete fibril formation is proportional to the film thickenss: $X_{rupt} \simeq H\tau_f/E$. While this displacement is being performed, stress remains constant ($\pi \simeq \tau_f/\kappa$) and this corresponds to a plateau in the stress-displacement curve. Once the entire film is turned into fibrils, the stress is still of the order of τ_f inside the fibrils themselves. Further elongation of the fibrils by a small factor is then possible, but soon the stress at the contact spots reaches τ_0, and the fibrils thus debond from probe. Correspondingly, the traction stress increases slightly and then soon vanishes. The energy that corresponds to the fibrillation mechanism can be estimated as

$$G \simeq X_{rupt}\tau_f/\kappa \simeq H\tau_f^2/\kappa E, \qquad (6)$$

which can be very high indeed: taking $E \simeq 2 \times 10^4$ Pa, $\tau_f \simeq 8 \times 10^4$ Pa, and $H \simeq 100\ \mu$m, one gets $G \simeq 16$ J/m^2.

With the usual roughness characteristics for a metal probe, one has $E < E^- \simeq 3 \times 10^6$ Pa, and therefore $\tau_0 \simeq p_0$ [Eq. (5)]: τ_f has to lie between p_0/κ and p_0,

in the present version of the model (zero applied contact pressure). For a much smoother probe (such as glass), one can have $E > E^-$ and much higher values of τ_0 and τ_f.

The most rewarding feature of the present model is that by taking into account both the film and the probe surface roughnesses and understanding the role of air suction, it was possible to obtain quantitative predictions both of the high tack energy [Eq. (6)] and of the maximum force necessary for separating the two surfaces ($\pi_{max} \simeq \tau_0/\kappa$). Such predictions can be tested using different parameters: elastic modulus of the polymer (e.g., by adjustable cross-linking [7]; see predictions on Fig. 5), surface interactions (e.g., by chemical treatment), film surface roughness (by varying the film deposition method), and even atmospheric pressure (in a controlled experiment) on a more microscopic scale. In the present Letter, we focused on soft, thick films ($E < E^\star$ and $H > D$) under zero applied pressure. Other regimes deserve a more thorough study and will be published separately. For instance, if pressure is applied in such a manner that air is driven away, the suction-cup effect will be more pronounced and a higher adhesion will be achieved. It will also be interesting to include viscoelastic effects which can be important to predict the dependence of the tack energy on contact time and debonding speed and for melts or weakly cross-linked materials often used in practical applications.

---

[1]   C. A. Dahlquist, in *Treatise on Adhesion and Adhesives*, edited by R. L. Patrick (Dekker, New York, 1969), p. 2.
[2]   R. J. Good and R. K. Gupta, J. Adhes. **26**, 13–36 (1988).
[3]   P.-G. de Gennes, C. R. Acad. Sci. **307**, 1949–1953 (1988).
[4]   P.-G. de Gennes, C. R. Acad. Sci. **312 II**, 1415–1418 (1991).
[5]   T. Ondarçuhu, J. Phys. II (France) **7**, 1893–1916 (1997).
[6]   A. Zosel, J. Adhes. **30**, 135–149 (1989), and references therein.
[7]   A. Zosel, J. Adhes. **34**, 201–209 (1991).
[8]   K. N. G. Fuller and D. Tabor, Proc. R. Soc. London A **345**, 327–342 (1975).
[9]   C. Creton and L. Leibler, J. Polym. Sci. B **34**, 545–554 (1996).
[10] K. L. Johnson, K. Kendall, and A. D. Roberts, Proc. R. Soc. London A **324**, 301 (1971).
[11] The transition at $E \approx E^\star$ can also be described as the percolation of the area of contact between the probe and the film: large contact spots merge into a continuous domain while, conversely, the continuous no-contact zone (air) turns into a set of disconnected spots (bubbles).
[12] L. Leibler (unpublished).